Microchemical Journal 193 (2023) 109079



Contents lists available at ScienceDirect

Microchemical Journal

journal homepage: www.elsevier.com/locate/microc





Electrochemical sensor for simultaneous determination of paracetamol, propyphenazone, and caffeine – Electrodes based on poly(L-cystine)/gold nanoparticles plating on pencil graphite

Ayça Urçuk, Ceren Yıldız, Dilek Eskiköy Bayraktepe, Zehra Yazan *

Ankara University, Faculty of Science, Department of Chemistry, 06560 Ankara, Turkey

ARTICLE INFO

Keywords:
Electrochemical nanosensor
Poly(L-cystine)
Gold nanoparticles
Paracetamol
Propyphenazone
Caffeine

ABSTRACT

An electrode based on pencil leads (PGE) coated with gold nanoparticles (AuNPs) and poly(L-cystine) (P(L-cyst)) was devised and used for the simultaneous analysis of ternary drug combinations, namely, paracetamol (PA), propyphenazone (PRO) and caffeine (CA). The sensor is designed step-by-step by electro-polymerization: P(L-cyst) plating on the surface of PGE and then electrodeposition of AuNPs. The electrode performance was investigated using cyclic voltammetry (CV). Changes on the electrode surface were elucidated by electrochemical impedance spectroscopy (EIS), field emission scanning electron microscopy (FE-SEM), and Energy Dispersive X-ray analysis (EDX). Compared to bare PGE, the modified sensor proved to be better in electrochemical current density for the analytes. The improvement was attributed to the synergistic effects of AuNPs and the organic matrix. The linear ranges were 0.023–90.0 μM (for PA), 0.009 – 30.0 μM (for PRO), and 0.454–600.0 μM (for CA). Trial studies were also done on real samples to reveal the accuracy and reproducibility of the method.

1. Introduction

The common non-steroidal drugs containing paracetamol, propyphenazone, and caffeine are anti-inflammatory drugs. They are household drugs used as analgesic, anti-inflammatory, and antipyretic agents [1,2]. These drugs are known to control fever caused by bacterial and viral infections [3]. There are some adverse effects of these combinations when consumed in excess dosage. These adverse effects include decreased red blood cells, breathing problems, skin rashes, facial swelling, nausea, dizziness, and liver damage [4–6].

Many analytical techniques, such as derivative spectrophotometry [7] and chromatography [8,9], have been used to analyze the mixtures of compounds in biological fluids and pharmaceuticals. In clinic applications and diagnostic research, a susceptible and accurate analysis method is required to detect these active ingredients simultaneously. In addition, a suitable analytical method is also required for the simultaneous analysis of multiple analytes in different fields, such as biomolecule analysis [10], environmental assay [11], and bacterial detection [12]. Analyzing multicomponent mixtures without separating the constituents is a rather difficult task. Because each analyte may require different conditions for an accurate analysis, spectrophotometric techniques may suffer from interferences due to overlapping the spectra of individual analytes interested or due to the presence of contaminations.

Electroanalytical methods have become popular in the determination of multiple analytes. These methods are generally less time-consuming, simple, fast, require low-cost instrumentation, and have low detection limits [13].

Various electroanalytical techniques for individual and dual determination of PA and CA have been reported [14,15]. The electrochemical oxidation peaks of PA, PRO, and CA proved highly reliable. However, the simultaneous identification of the three compounds is a more significant challenge due to their close oxidation potentials. Consequently, developing a simple, single-use, sensitive, selective, precise, and low-cost alternative voltammetric method is desirable.

Pencil graphite electrodes (PGEs) are customarily used as working electrodes. They are cheap, easy to use, and suitable for surface modification. In recent years, the surface of PGEs has been modified with some modifiers such as metal nanoparticles [16,17], carbon nanotubes [18,19], and conducting polymer films [20] to improve the selectivity and sensitivity. Treating the electrode surfaces with conducting polymers and metal nanoparticles improves electrocatalytic activity on the modified electrodes. For example, gold metal nanoparticles (AuNPs) can be used for electrochemical sensing platforms due to their excellent biological compatibility, large surface-to-volume ratio, active sites, and

* Corresponding author.
E-mail address: zdurmus@science.ankara.edu.tr (Z. Yazan).

https://doi.org/10.1016/j.microc.2023.109079
Received 28 April 2023; Received in revised form 7 July 2023; Accepted 9 July 2023
Available online 10 July 2023
0026-265X/© 2023 Elsevier B.V. All rights reserved.

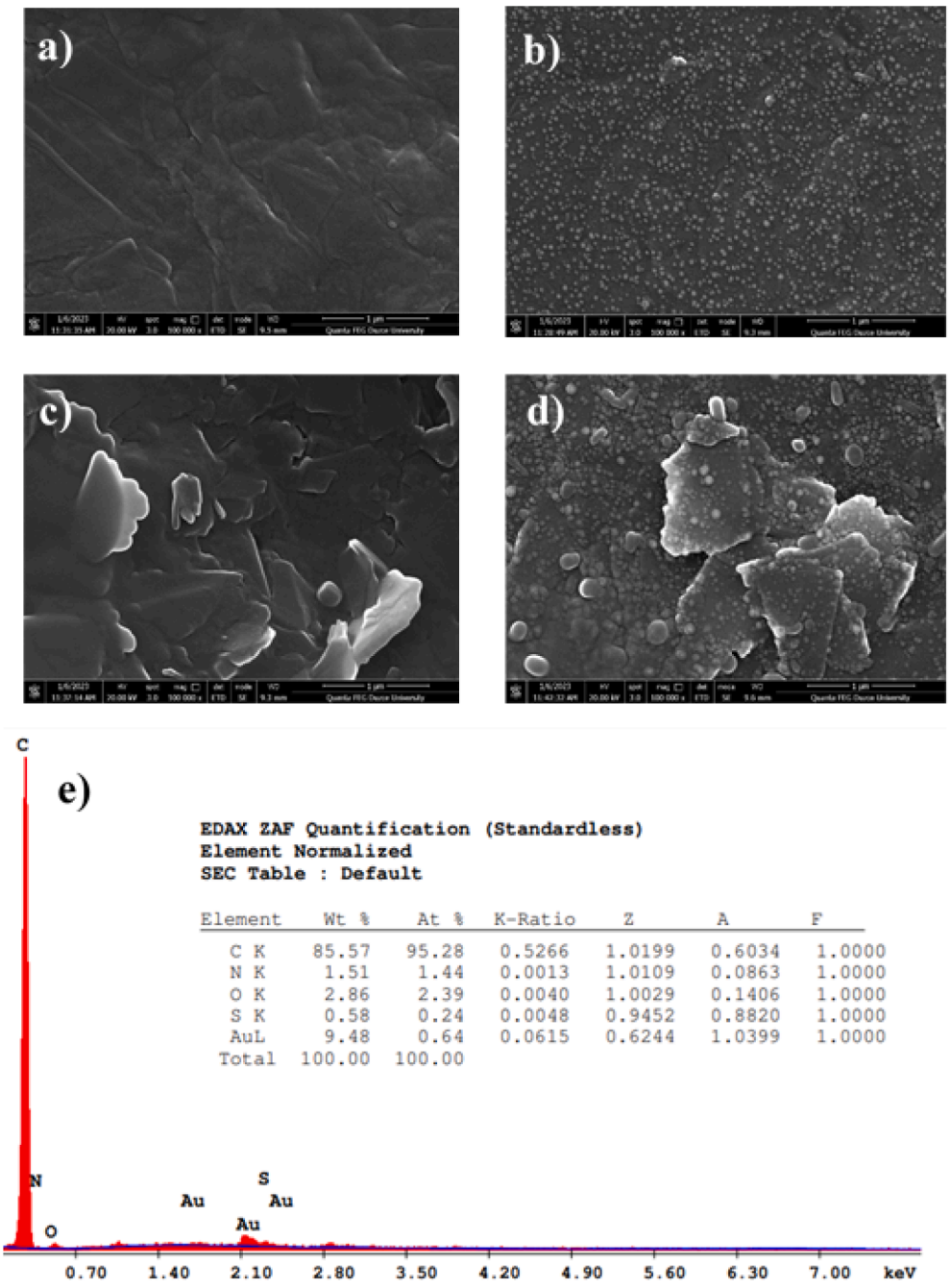

Fig. 1. FE-SEM images of a) PGE, b) AuNPs/PGE, c) P(L-cyst)/PGE, d) P(L-cyst)/AuNPs/PGE, and e) EDX spectrum of P(L-cyst)/AuNPs/PGE.

high catalytic activity [21].

Another treatment for improving electrode performance is polymerizing some biochemical molecules on the electrode surfaces, thereby changing their conductivity, stability, and doped properties. Poly(amino acids) is an example of such polymer, and they can be formed on the electrode surface concomitantly or before metal nanoparticle coating. These polymers, with their porous structures, can also serve as a matrix in the attachment of metal nanoparticles onto the electrode surface and thus create more electrocatalytic sites [20].

The sulfur-containing amino acids, L-cysteine and L-cystine, can be polymerized electrochemically on the electrode surfaces to modify the electrochemical sensor. Of these two amino acids, L-cysteine has been used widely to improve electrochemical analyses [22,23]. However, papers reporting using L-cystine (L-cyst) as a modifier are far less frequent. As L-cyst contains disulfide bonds (S-S), some differences between its polymers and the polymers of L-cysteine could be expected because the S-S moiety is likely to form stable coordination bonds with gold atoms. Due to the characteristic complexing power of the S-S group, poly (disulfide) polymers find a wide range of uses as drug-carrier systems [24,25] and energy storage agents [26].

In this work, we modified pencil graphite electrode surfaces by electro-polymerizing L-cystine and then electrodeposition of gold from a solution of $HAuCl_4$. The modified electrode (P(L-cyst)/AuNPs/PGE) was used to quantify PA, PRO, and CA in ternary mixtures simultaneously. The optimization studies of the modified electrode were also carried out. The morphology and electrochemical characteristics of the composite electrode surface were investigated using FE-SEM, EDX, EIS, and CV. The P(L-cyst)/AuNPs/PGE- electrode devised proved to be a versatile tool in a wide range of concentrations. The detection limits are satisfactory. The applicability of the method was tested in biological and

pharmaceutical samples.

2. Experimental

2.1. Reagents and instruments

Paracetamol, propyphenazone, and caffeine were supplied from ATABAY Drug Company, Istanbul, Turkey. 0.01 M stock solutions of PRO and CA were prepared by dissolving known amounts of drug ingredients in the methanol–water mixture (1:1), and 0.01 M aqueous stock solution of PA was used to prepare the calibration solutions. Analytical grade L-cystine, $HAuCl_4{\cdot}3H_2O$, H_3PO_4, CH_3COOH, H_3BO_3, HCl, NaOH, and C_2H_5OH were purchased from Sigma Aldrich. 0.1 M Britton-Robinson buffer (BR) with different pH values was prepared by adding appropriate amounts of CH_3COOH, H_3PO_4, and H_3BO_3. The pH values of the final solutions for analysis were adjusted by adding 0.01 M HCl or 0.01 M NaOH. Human serum samples were obtained from Sigma Aldrich. Electrochemical measurements were performed with a PalmSens*4* potentiostat/galvanostat. In ambient conditions, pH measurements were done using a HANNA HI2211 model pH/ORP meter.

The surfaces of sensors were investigated using FE-SEM images, and EDX data was obtained on the instrument Energy Dispersive Quanta FEG 250 model (FEI, Holland). An acceleration voltage of 20 KeV was applied for the FE-SEM images.

2.2. Electrode preparation

2.2.1. Electrochemical polymerization of L-cystine

The P(L-cyst)/AuNPs/PG electrode was prepared in two steps: the electro-polymerization of the L-cyst and the electrodeposition of gold nanoparticles. A monomer solution (0.1 mM L-cyst) was prepared in 0.1 M phosphate buffer, PBS (pH 7.0), for the first step. 10.0 mL of the buffered solution was placed in the working cell. Nitrogen gas was passed through the cell for 5 min before the electrochemical polymerization. Cyclic voltammetry was used for the polymerization in the potential range (−0.5) to (+1.8) V with a scan rate of 75 mVs^{-1} for ten cycles. Finally, the electrode was rinsed with distilled water to remove any unbound material on the surface.

The typical redox behavior related to polymer in the first cycle is observed at 1.30 V potential (Supplementary Fig. S1) [27]. The high peak current is tentatively attributed to the coupling of radical cations to form the polymer. In the repetitive cycles, the cation radicals combine to form dimers, oligomers, and finally, the polymer film on the electrode surface − the increase in the number of cycles caused an increase in the current intensities. The polymerized electrode was then dried at ambient temperature.

2.2.2. Electrodeposition of Au nanoparticles on the polymer-coated electrode

The polymer-coated pencil graphite electrode was coated with Au nanoparticles via an electrochemical deposition process using the CV technique. The deposition was achieved from a solution containing 0.05 mM $HAuCl_4$ in 0.01 M H_2SO_4 solution. The coating was performed in the potential range (−0.2) − (+1.3) V at 50 mVs^{-1} scan rate (Fig. S2) [28].

The parameters (cycle number, the concentration of $HAuCl_4$, and L-cystine) were optimized to achieve the highest peak currents with the three analytes. CV trials, EIS, and SEM-EDX images characterized the electrode surface so modified.

2.3. Electrochemical measurements

Square wave voltammetry (SWV), EIS, and CV measurements were performed using a PalmSens*4* potentiostat/galvanostat (from Holland). A BAS C3 cell-stand system (Bioanalytical Systems, Inc., USA) was used in connection. This electrode system consists of a platinum wire (Pt), a PGE, and an Ag/AgCl electrode as counter, working, and reference electrodes, respectively. SWV method was selected due to the minimal contribution of nonfaradaic currents. The SWV parameters were adjusted by optimization as step height 0.005 V, amplitude 0.025 V, and frequency 25.0 Hz.

2.4. Real samples

Human serum was obtained from Sigma Aldrich Company (H4522, from human male AB plasma, USA origin, sterile-filtered). Serum samples were stored at −20 °C and used without any pre-treatment. For the preparation of samples, the known concentrations of analytes were spiked into a human serum sample containing 0.01 M H_2SO_4 solution. This stock solution was used for calibration and recovery studies. The standard addition method was employed. Five PAROL Plus tablets (each tablet contains 250 mg, 150 mg, and 50 mg of PA, PRO, and CA) were weighed and finely powdered in a porcelain mortar. The adequate amounts of the powdered tablets corresponding to a 1.6×10^{-2} M PA, 6.0×10^{-3} M PRO, and 2.0×10^{-3} M CA were transferred to a 100 mL volumetric flask and prepared with deionized water and methanol (1:1). The mixture was sonicated for 15 min. After the excipients settled, known volumes of the clear supernatant solution were transferred to a 10 mL voltametric cell containing 0.01 M H_2SO_4 solution. The voltammograms were recorded under the optimum experimental conditions.

3. Results and discussion

3.1. Surface morphology of the electrodes

The surfaces of the electrodes were investigated by the FE-SEM method. The morphologies of the modified PGEs are given in Fig. 1. The surface of bare PGE is regular, smooth, and homogenous as expected (Fig. 1a). Gold nanoparticles of spherical shape were evenly scattered on AuNPs/PGE electrode (Fig. 1b).

After the electro-polymerization of L-cyst on the bare PGE (Fig. 1c), the surface changes indicate that L-cystine polymerization did occur. Fig. 1d represents the surface of P(L-cyst)/AuNPs/PGE, which appears to have a tight polymer network. The EDX spectrum of the P(L-cyst)/AuNPs/PGE nanocomposite (Fig. 1e) also contains Au, N, S, C, and O atoms.

3.2. Optimization of the P(L-cyst)/AuNPs/PGE sensor

The optimum values for the concentrations of L-cyst and $HAuCl_4$ used in the surface treatment, the number of cycles, and the scan rates applied in L-cystine polymerization were determined. The results are shown in Figs. S3 and S4. L-cyst concentrations were changed between 0.1 mM and 1.0 mM, with $HAuCl_4$ concentrations kept constant at 0.05 mM. As the concentration of L-cyst increased in the range of 0.1 mM − 1.0 mM, a decrease was observed in the analyte's anodic peak currents. This was attributed to surface saturation (Fig. S3a). For the best separation of the analyte peak potentials with the lowest background currents, 0.1 mM of L-cyst was selected as the optimum value because higher L-cyst concentrations cause a decrease in the peak currents of the three analytes (Fig. S3a). The concentration of $HAuCl_4$ was changed in seven different concentrations in the range of 0.01 mM – 0.5 mM with L-cyst fixed at 0.1 mM. The optimum $HAuCl_4$ concentration was 0.05 mM (Fig. S3b).

Electro-polymerization and electrodeposition procedures were also optimized. In this context, the effect of the number of CV cycles and scan rates was investigated. The number of cycles was arranged between 5 and 30 with increments of 5 cycles (Fig. S4a, b). The optimum cycle number was found to be 10. As seen in Fig. S4a, the peak currents of PA and CA remain almost the same as the number of CV cycles changes. However, the peak current of PRO decreases as the number of cycles increases. Presumably, more than ten cycles cause a decrease in the number of active sites on the polymer/Au coating. The electrode surface

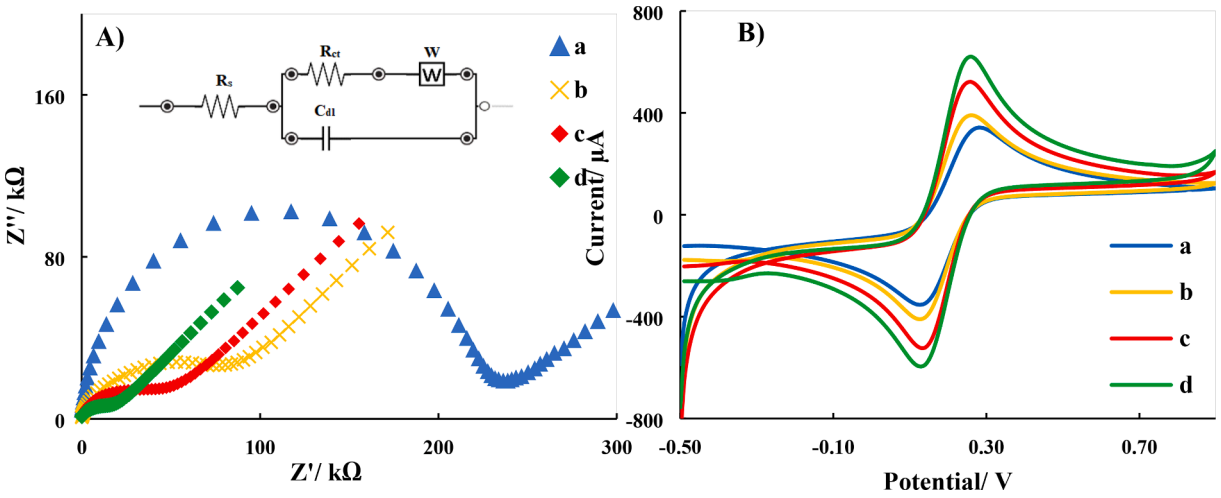

Fig. 2. A) Nyquist diagrams, B) Cyclic voltammograms of (a) PGE, (b) P(L-cyst)/PGE, (c) AuNPs/PGE, and (d) P(L-cyst)/AuNPs/PGE in 0.1 M KCl solution containing 5.0 mM of 1:1 $[Fe(CN)_6]^{3-}$ and $[Fe(CN)_6]^{4-}$ mixture at a scan rate of 0.05 Vs^{-1}. (W: Warburg element, R_s: the cell resistance, R_{ct}: Charge transfer resistance, C_{dl}: The capacitance of the double layer).

was coated by changing the scan rate in the range of 25.0 – 125 mVs^{-1} with increments of 25 mVs^{-1}. The best scan rates were 75 mVs^{-1} and 50 mVs^{-1}, respectively, for L-cyst and AuNPs, (Fig. S4c, d).

3.3. Electrochemical characterization

The EIS technique evaluated the modified electrodes' charge transfer resistance (R_{ct}). The experiments were performed at a frequency range of 0.01 Hz – 100 kHz using a redox probe of 5.0 mM of $[Fe(CN)_6]^{3-}$ and $[Fe(CN)_6]^{4-}$ [a] mixture containing 0.1 M KCl (the open circuit potential: 0.237 V). The Nyquist plots in Fig. 2A represent a) PGE, b) P(L-cyst)/PGE, c) AuNPs/PGE, and d) P(L-cyst)/AuNPs/PGE. The impedance spectra given in Fig. 2A were fitted with the same electrical equivalent circuit by Z Circuit Fitting software in Palmsen*4* and given in the inset of Fig. 2A. This equivalent circuit model consists of R_{ct}, the charge transfer resistance representing high-frequency region, serially connected Warburg element (W) (representing the low-frequency region) and R_s, the cell resistance, and C_{dl}, the capacitance of the double layer, connected in parallel with W and R_{ct}. The connection of the whole system was as given in Fig. 2A inset.

The fitting results of electrical circuit elements were given in Table S1 for bare and modified sensor surfaces. A comparison of the experimental results with different R_{ct} values indicates that the smallest R_{ct} was obtained using P(L-cyst)/AuNPs/PGE. It could be attributed to the fact that the conductivity of the P(L-cyst)/AuNPs/PGE electrode is higher than that of the bare PGE surface, leading to a lower electron transfer resistance.

The four electrodes were also characterized using the CV method with the same electrode at a scan rate of 50 mVs^{-1}. The result is shown in Fig. 2B. ΔE_p values for the P(L-cyst)/AuNPs/PGE were lower than those obtained with the other electrodes.

The surface area of the electroactive part of the electrode was calculated using the Randles-Sevcik equation [29].

The surface areas were (0.75 ± 0.03) cm^2, (0.69 ± 0.03) cm^2, (0.67 ± 0.01) cm^2 and (0.63 ± 0.02) cm^2 for P(L-cyst)/AuNPs/PGE, AuNPs/PGE, P(L-cyst)/PGE and PGE, respectively. The surface area of P(L-cyst)/AuNPs/PGE is remarkably larger than others. The CV data confirm the results of EIS.

3.4. Preliminary SWV studies

The SWV electrochemical responses of PA, PRO, and CA obtained with P(L-cyst)/AuNPs/PGE, AuNPs/PGE, P(L-cyst)/PGE, and PGE are shown in Fig. 3. The peak currents of PA, PRO, and CA obtained with bare PGE are the weakest. After modification with P(L-cyst)/AuNPs, the oxidation peak currents increase by about 80%. The peak potentials shift to negative values (particularly for PRO and CA), indicating that the oxidation processes of the analytes proceed more easily on the surface of the electrode.

3.5. CV studies

For a further investigation of the electrochemical behavior of the analytes, individual CV voltammograms of PA, PRO, and CA were taken (Fig. S5). PA has a sharp anodic peak at 0.61 V and a cathodic peak at 0.66 V, and PA has a quasi-reversible redox process. Similarly, CV voltammograms of PRO and CA show an irreversible redox process with anodic peaks at 1.10 V and 1.50 V, respectively. The process involves the loss of two electrons and two protons, which means the oxidation of paracetamol to N-acetyl-p-quinone imine species [30]. No reduction peak was observed for PRO and CA in the reverse scan. CA is known to be oxidizable by losing four electrons and four protons in the pH range of 1.0 to 3.5 [15]. On the other hand, the electrochemical oxidation of PRO is reported to occur with the loss of one electron per molecule [31].

3.5.1. Scan rate studies

Cyclic voltammograms at different scan rates (25 mVs^{-1} —1000 mVs^{-1}) were recorded. The plot showing the peak currents (i_p) versus the square root of scan rate ($\upsilon^{1/2}$) was obtained. The linear relation between i_p and $\upsilon^{1/2}$ indicated a diffusion behavior of electro-oxidations of PA and CA at modified P(L-cyst)/AuNPs/PGE electrode surface. However, a nonlinear relation was observed for PRO, indicating a mechanism not governed by diffusion. The log i_p – logυ plots for the three analytes are given in the insets of Fig. S6. The slope of logi_p vs. logυ for PRO (0.88) indicates that the electrode reaction is controlled by adsorption (Fig. S6 inset b) [32]. The slope values are close to 0.5 for PA and CA.

3.6. The studies on the pH effects

pH adjustments are often employed in the quantitative electrochemical analysis of multiple analytes simultaneously. Changes in the pH value influence the peak currents and peak potentials of analytes because of the involvement of protons in the oxidation reactions [33]. The effect of pH on the oxidation peak currents and potentials of PA, PRO, and CA was investigated by the SWV method in the pH range from

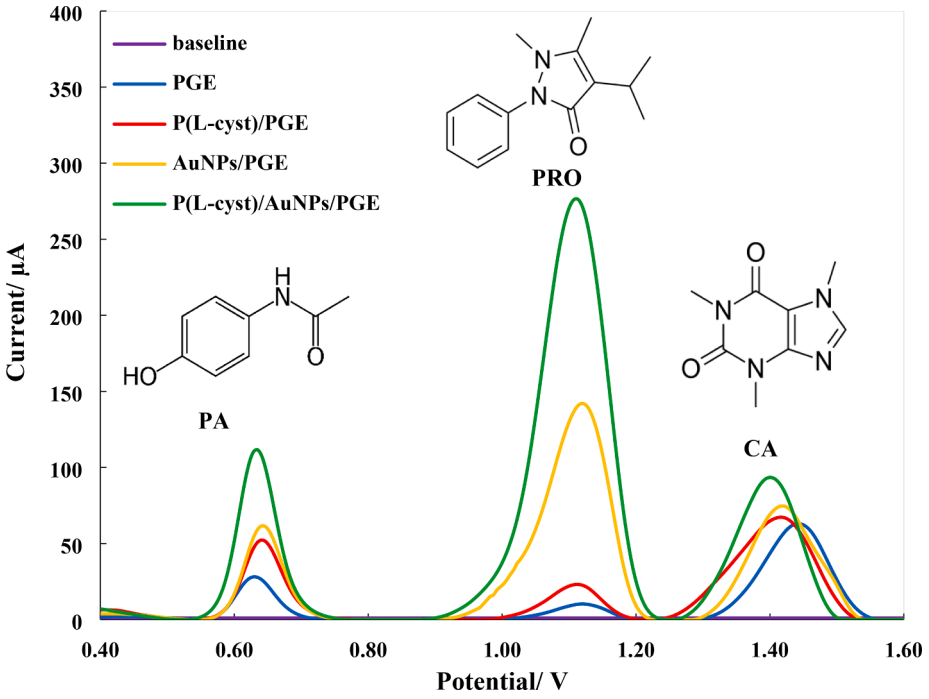

Fig. 3. SWV voltammograms of the different modified PGE sensors for 100.0 µM PA, 10.0 µM PRO, and 500.0 µM CA in 0.01 M H_2SO_4 solution, pH 2.0.

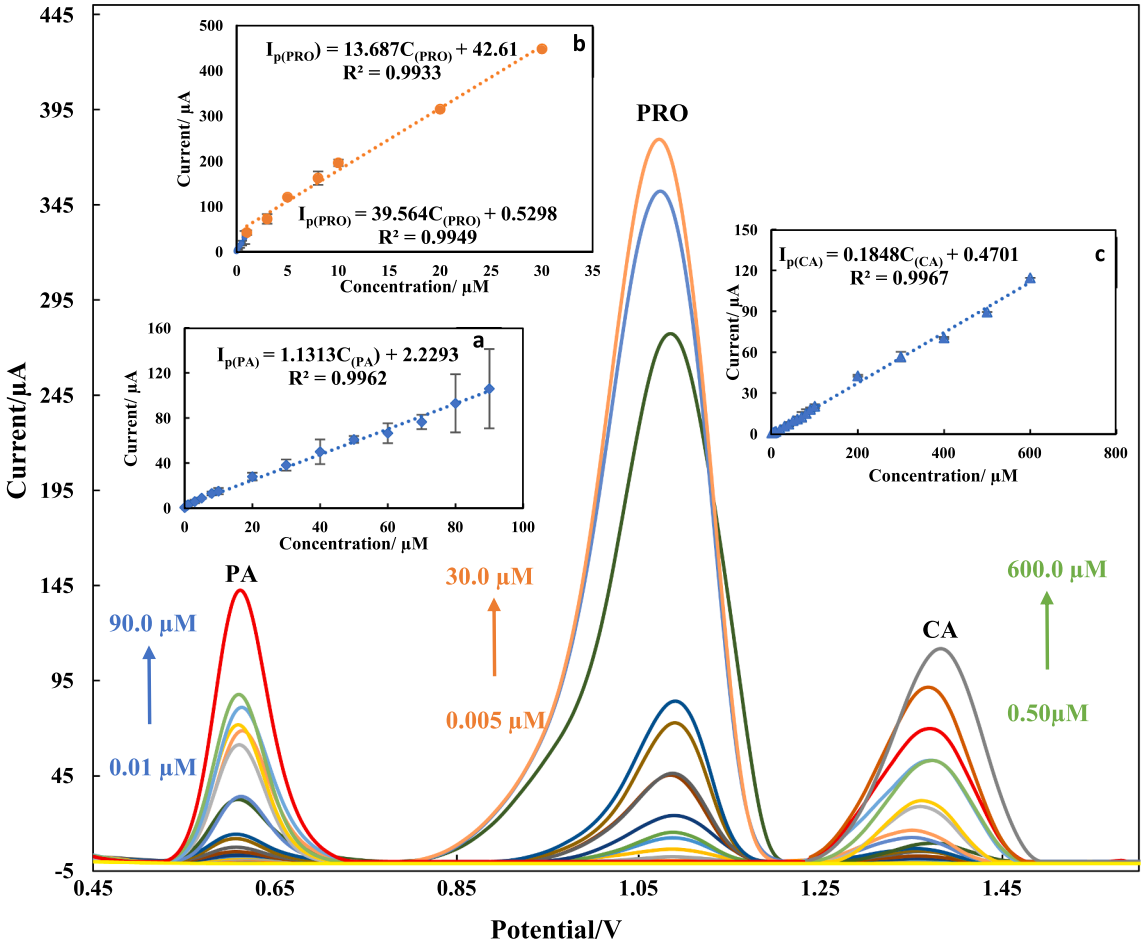

Fig. 4. SWVs of simultaneous PA PRO and CA determination using P(L-cyst)/AuNPs/PGE electrode in 0.01 M H_2SO_4 (pH 2.0). **Insets:** Plots of peak current vs. a) PA, b) PRO, and c) CA concentrations.

Table 1
Regression data relating to the simultaneous calibration lines of PA, PRO, and CA on P(L-cyst)/AuNPs/PGE sensor.

Regression parameters	PA	PRO	CA
Linear working range, μM	0.023 – 90.0	0.009 – 1.0; 1.0 – 30.0	0.454 – 600.0
Limit of detection (LOD), μM	0.007	0.003	0.136
Limit of quantification (LOQ), μM	0.023	0.009	0.454
Regression coefficient (R^2)	0.9962	0.9949; 0.9933	0.9967
Reproducibility of peak potential, RSD%[a]	0.49	1.52	0.74
Reproducibility of peak current, RSD%[a]	1.02	2.07	1.97
Repeatability of peak potential, RSD %[a] (inter-days)	0.11	0.13	0.34
Repeatability of peak current, RSD %[a] (inter-days)	2.64	0.64	2.47
Repeatability of peak potential, RSD %[a] (intra-day)	0.74	0.18	0.16
Repeatability of peak current, RSD %[a] (intra-day)	2.80	2.34	1.13

[a] RSD is the relative standard deviation of 5 replications.

2.0 to 7.0 with various supporting electrolytes and buffer solutions to select the optimum pH and supporting electrolyte for the suited oxidation peaks of PA, PRO, and CA (Fig. S7). The maximum peak currents were obtained in 0.01 M H_2SO_4 (pH 2.0) supporting electrolytes. In addition, the peak potentials of PA and CA shifted to positive potential values with increased pH values. This shift indicates the involvement of proton(s) in the electrochemical oxidation reaction of PA and CA. The peak potential of PRO was relatively constant (Fig. S7 inset b). This result showed that the electro-oxidation mechanism of PRO is not pH-dependent [31].

3.7. Simultaneous analysis of PA, PRO, and CA

PA, PRO, and CA quantitation was investigated using P(L-cyst)/AuNPs/PGE with the SWV method. The analytes were added to the medium at various concentrations. The optimized conditions found beforehand were applied (Fig. 4). The i_p vs. concentrations relations for the three biomolecules were obtained in ranges 0.01 – 90.0 μM (for PA), 0.05 – 30.0 μM (for PRO) and 0.50 – 600.0 μM (for CA).

Validation parameters are represented for ternary detection of PA, PRO, and CA in Table 1. The limit of detection (LOD, 3 s/m) and limit of quantification (LOQ, 10 s/m) were found using the linear curves, where s is the standard deviation in peak current values found for the lowest concentrations of analytes and m is the slope of the calibration plot). For PA, PRO, and CA, the detection limits were 0.007 μM, 0.003 μM, and 0.136 μM, and the LOQ values were 0.023 μM, 0.009 μM, and 0.454 μM, respectively. These results showed that the sensor exhibited excellent repeatability and reproducibility values.

The stability of the P(L-cyst)/AuNPs/PGE sensor was tested by conducting 50 repetitive measurements using a single P(L-cyst)/AuNPs/PGE sensor in 5.0 mM of $[Fe(CN)_6]^{3-/4-}$ mixture solution at a scan rate of 0.05 Vs^{-1}. The related CV voltammograms are given in Fig. S8a. As can be seen, the sensor displays stable anodic and cathodic currents and stable potential responses. Besides, the RSD% values for anodic and cathodic peak currents are 1.12% and 0.92%, respectively. Moreover, the stability of the sensor was tested with the analyte solution containing 1.0 μM PA and PRO; 10.0 μM CA (Fig. S8b). The RSD% values of 5 repetitive current responses for all analytes were below 5%, confirming the sensor's stability for simultaneous PA, PRO, and CA analysis of at least five measurements.

The sensor's performance was compared with those of other reported modified electrodes (Table 2). As seen, the performance of the modified sensor is comparable to those used in previous works.

Table 2
Comparison of the performance of P(L-cyst)/AuNPs/PGE sensor with the literature data.

Electrode	Method	Analyzed compounds	Working Ranges (μM)	LOD (μM)	Sample	Lit.
SWCNT/CCE	DPV	**PA**	0.08 – 200.0	0.05 0.29	Drinking and biological samples	[34]
		CA	0.41 – 300.0			
poly(AHNSA)/GCE	SWV	**PA**	10.0 – 125.0	0.45	Coca-cola, Pepsi-Cola, and Tea Samples	[35]
		CA	10.0 – 125.0	0.79		
Bi/Nafion/BDDE	DPV	**PA**	0.20 – 500.0	0.036	Pharmaceutical extract and Energy drink	[36]
		CA	0.01 – 20.0	0.0028		
BDD	SWV	**PA**	6.6 – 330.8	0.060	–	[31]
		PRO	4.3 – 217.1	0.022		
		CA	5.2 – 205.98	0.031		
BDD	BIA-SWV	**PA**	13.2 – 330.8	1.98	–	[31]
		PRO	8.7 – 217.1	0.87		
		CA	10.3 – 257.5	1.54		
MOF-199/Naf-GCE	DPV	**PA**	0.10 – 5.0	1.26	Pharmaceutical preparations	[37]
		CA	0.20 – 5.0	1.24		
aGCE	SWV	**PA**	10.0 – 180.0	2.55	Pharmaceutical samples	[38]
		CA	10.0 – 95.0	2.36		
3D-printed sensor	DPV	**PA**	0.66 – 40.0	2.84	Urine sample	[14]
		CA	0.37 – 220.0	2.01		
GrRAC	DPV	**PA**	0.0 – 50.0	2.01	Pharmaceuticals in dosage forms and synthetic urine	[39]
		CA	0.0 – 50.0	2.31		
GrRGC	DPV	**PA**	0.0 – 50.0	4.23	Pharmaceuticals in dosage forms and synthetic urine	[39]
		CA	0.0 – 50.0	6.33		
P(L-cyst)/AuNPs/PGE	*SWV*	***PA***	*0.023 – 90.0*	*0.007*	*Biological and pharmaceutical samples*	***Present Work***
		PRO	*0.009 – 1.0; 1.0 – 30.0*	*0.003*		
		CA	*0.454 – 600.0*	*0.136*		

SWCNT/CCE: Single-walled carbon nanotubes modified carbon-ceramic electrode; poly(AHNSA)/GCE: poly(4-amino-3-hydroxynaphthalene sulfonic acid)-modified glassy carbon electrode; Bi/Nafion/BDDE: Bismuth particles nafion covered boron-doped diamond electrode; BDD: Boron-doped diamond electrode; MOF-199/Naf-GCE: Metal organic frameworks based nafion-glassy carbon electrode; aGCE: activated glassy carbon electrode; GrRAC: Raw cork modified graphite electrode; GrRGC: Regranulated cork modified graphite electrode; P(L-cyst)/AuNPs/PGE: Pencil graphite electrode modified with gold nanoparticles and poly(L-cystine).
PA: Paracetamol; PRO: Propyphenazone; CA: Caffeine; DPV: Differential pulse voltammetry; SWV: Square wave voltammetry; BIA-SWV: Batch injection analysis-Square wave voltammetry.

Table 3
Recovery results in pharmaceutical dosage and human serum samples.

Real Sample	Method	Sample	Added amount, μM	Found amount, μM	Average recovery, %	RSD[a], %
Pharmaceutical dosage form	SWV	PA	10.0	10.21 ± 0.2906	102.07 ± 2.91	2.85
		PRO	10.0	10.14 ± 0.3759	102.93 ± 3.69	3.58
		CA	3.0	3.04 ± 0.0564	100.96 ± 1.18	1.86
Human serum sample	SWV	PA	1.0	0.97 ± 0.0073	96.76 ± 0.73	0.75
		PRO	1.0	0.99 ± 0.0132	99.87 ± 1.32	1.32
		CA	1.0	1.04 ± 0.0105	103.97 ± 1.06	1.02

[a] Each value is the mean of three experiments (95% Confidence Level).

3.8. Interference study

The effect of various possible interfering agents in biological samples, dopamine, glucose, caffeine, glycine, ascorbic acid, and uric acid, was investigated. These studies showed that these compounds did not significantly affect the performance of the P(L-cyst)/AuNPs/PGE sensor with a relative error of less than ± 10.0%. The relative errors were calculated based on the difference between initial and subsequent current responses of PA, PRO, and CA. The tolerance limits are only applicable under the conditions that the molar concentrations of the interfering species do not exceed that of the analytes, PA, PRO, and CA (1:1). The relative error caused by each species was always below 4.0% (Fig. S9).

3.9. Application

To test the analytical applicability and reliability of the proposed electrode, we spiked human serum into the solution containing analytes. Then, the analytes were analyzed from the pharmaceutical sample with the standard addition method. The recovery results are presented in Table 3. Clearly, PA, PRO, and CA recoveries are satisfactory.

4. Conclusion

A new P(L-cyst)/AuNPs/PGE-based electrochemical sensor was developed to quantify PA, PRO, and CA in human serum and pharmaceutical samples simultaneously. The combined properties of AuNPs and poly(L-cyst) formed a remarkable electrocatalytic oxidation of PA, PRO, and CA. The characterization and electrochemical properties of the P(L-cyst)/AuNPs/PGE sensor were performed via FE-SEM/EDX, CV, and EIS techniques. The sensor demonstrated great sensitivity, precision, accuracy, and reproducibility for the electro-analysis of the ternary mixture. The linear concentration ranges were (0.023 – 90.0) μM (for PA), (0.009 – 1.0; 1.0 – 30.0) μM (for PRO), and (0.454 – 600.0) μM (for CA). Recovery studies showed the acceptability of sensors in human serum and pharmaceutical samples. The nanosensor provides an alternative to other sensors for quantifying drug combination preparations, biological samples, and different matrix mixtures.

CRediT authorship contribution statement

Ayça Urçuk: Investigation, Data curation. **Ceren Yıldız:** Investigation, Data curation. **Dilek Eskiköy Bayraktepe:** Resources, Investigation, Data curation, Writing – review & editing. **Zehra Yazan:** Supervision, Conceptualization, Methodology, Validation, Funding acquisition, Writing – review & editing.

Declaration of Competing Interest

The authors declare that they have no known competing financial interests or personal relationships that could have appeared to influence the work reported in this paper.

Data availability

Data will be made available on request.

Acknowledgments

The authors thank the Ankara University Research Fund (Project numbers 16L0430002, 20B0430003, and 17H0430009) for the financial support.

Appendix A. Supplementary data

Supplementary data to this article can be found online at https://doi.org/10.1016/j.microc.2023.109079.

References

[1] H. Kraetsch, T. Hummel, J. Lötsch, R. Kussat, G. Kobal, Analgesic effects of propyphenazone in comparison to its combination with caffeine, Eur. J. Clin. Pharmacol. 49 (1996) 377–382, https://doi.org/10.1007/BF00203781.
[2] K. Delvadiya, P. Kabra, R. Kimbahune, N. Patel, L. Nargund, High-performance Liquid Chromatographic Determination of Paracetamol, Propyphenazone, and Caffeine in Pharmaceutical Formulations, Indian J. Pharm. Educ. Res. 47 (4) (2013) 65–72, https://doi.org/10.5530/ijper.47.4.9.
[3] F. Soponar, D. Staniloae, G. Moise, B. Szaniszlo, V. David, Simultaneous determination of paracetamol, propyphenazone, and caffeine from pharmaceutical preparations in the presence of related substances using a validated HPLC-DAD method, Rev. Roum. Chim. 58 (4–5) (2013) 433–440.
[4] I. Popiołek, K. Piotrowicz-Wójcik, G. Porebski, Hypersensitivity reactions in serious adverse events reported for paracetamol in the EudraVigilance database, 2007–2018, Pharm. 7 (1) (2019) 12, https://doi.org/10.3390/pharmacy7010012.
[5] V. Boerlin, B. Maeglin, W. Hägler, M. Kuhn, E. Nüesch, Analgesic activity of propyphenazone in patients with pain following oral surgery, Eur. J. Clin. Pharmacol. 31 (1986) 127–131, https://doi.org/10.1007/BF00606648.
[6] A. Proudfoot, N. Wright, Acute paracetamol poisoning, Br. Med. J. 3 (5722) (1970) 557–558, https://doi.org/10.1136/bmj.3.5722.557.
[7] K. Srinivasan, J. Alex, A. Shirwaikar, S. Jacob, M.S. Kumar, S. Prabu, Simultaneous derivative spectrophotometric estimation of aceclofenac and tramadol with paracetamol in combination solid dosage forms, Indian J. Pharm. Sci. 69 (4) (2007) 540, https://doi.org/10.4103/0250-474X.36941.
[8] A. Saadatmandi, M.R. Sohrabi, H.K. Fard, Smart chemometrics spectrophotometry for rapid simultaneous quantitative determination of paracetamol, diphenhydramine, and phenylephrine in commercial tablet compared to high-performance liquid chromatography as a reference method, Chemom. Intell. Lab. Syst. 233 (2023), 104732, https://doi.org/10.1016/j.chemolab.2022.104732.
[9] H. Ibrahim, A.M. Hamdy, H.A. Merey, A.S. Saad, Simultaneous determination of paracetamol, propyphenazone, and caffeine in presence of paracetamol impurities using dual-mode gradient HPLC and TLC densitometry methods, J. Chromatogr. Sci. 59 (2) (2021) 140–147, https://doi.org/10.1093/chromsci/bmaa088.
[10] L.-X. Feng, C. Tang, X.-X. Han, H.-C. Zhang, F.-N. Guo, T. Yang, J.-H. Wang, Simultaneous and sensitive detection of multiple small biological molecules by microfluidic paper-based analytical device integrated with zinc oxide nanorods, Talanta 232 (2021), 122499, https://doi.org/10.1016/j.talanta.2021.122499.
[11] N.V. Kulagina, M.E. Lassman, F.S. Ligler, C.R. Taitt, Antimicrobial peptides for detection of bacteria in biosensor assays, Anal. Chem. 77 (19) (2005) 6504–6508, https://doi.org/10.1021/ac050639r.
[12] J.C. Jokerst, J.A. Adkins, B. Bisha, M.M. Mentele, L.D. Goodridge, C.S. Henry, Development of a paper-based analytical device for colorimetric detection of select foodborne pathogens, Anal. Chem. 84 (6) (2012) 2900–2907, https://doi.org/10.1021/ac203466y.
[13] N. Jadon, R. Jain, S. Sharma, K. Singh, Recent trends in electrochemical sensors for multianalyte detection–A review, Talanta 161 (2016) 894–916, https://doi.org/10.1016/j.talanta.2016.08.084.
[14] V. Katseli, A. Economou, C. Kokkinos, A novel all-3D-printed cell-on-a-chip device as a useful electroanalytical tool: Application to the simultaneous voltammetric

determination of caffeine and paracetamol, Talanta 208 (2020), 120388, https://doi.org/10.1016/j.talanta.2019.120388.
[15] B. Habibi, M. Abazari, M.H. Pournaghi-Azar, A carbon nanotube modified electrode for determination of caffeine by differential pulse voltammetry, Chinese J. Catal. 33 (11–12) (2012) 1783–1790, https://doi.org/10.1016/S1872-2067(11)60438-5.
[16] H.R.A. Hasanjani, K. Zarei, DNA/Au-Pt bimetallic nanoparticles/graphene oxide-chitosan composites modified pencil graphite electrode used as an electrochemical biosensor for sub-picomolar detection of anti-HIV drug zidovudine, Microchem. J. 164 (2021), 106005, https://doi.org/10.1016/j.microc.2021.106005.
[17] Ü.N. Tüzün, C. Yıldız, D. Eskiköy Bayraktepe, K. Polat, Z. Yazan, Electrochemical fabrication of poly (l-alanine)-gold nanoparticle nanocomposite-modified electrode: application for determination and mechanism of antipsychotic drug olanzapine, Monatsh. Chem. 154 (1) (2023) 95–104.
[18] Z.Q. Gong, A.N.A. Sujari, S. Ab Ghani, Electrochemical fabrication, characterization and application of carboxylic multi-walled carbon nanotube modified composite pencil graphite electrodes, Electrochim. Acta 65 (2012) 257–265, https://doi.org/10.1016/j.electacta.2012.01.057.
[19] C. Yıldız, D.E. Bayraktepe, Z. Yazan, Preparation of Multiwalled Carbon Nanotubes: Electrochemically Treated Pencil Graphite Electrodes for Nanomolar Detection of L-Tryptophan in Complex Samples, ChemistrySelect 7 (40) (2022) e202201697.
[20] D.E. Bayraktepe, Z. Yazan, Two-layered Au@ Ag Bimetallic Nanocomposites-poly (L-Met) Platform for Highly Sensitive Chlorpheniramine Maleate Detection, Electroanalysis 34 (3) (2022) 445–454, https://doi.org/10.1002/elan.202100422.
[21] S. Guo, E. Wang, Synthesis and electrochemical applications of gold nanoparticles, Anal. Chim. Acta 598 (2) (2007) 181–192, https://doi.org/10.1016/j.aca.2007.07.054.
[22] B.R.L. Ferraz, F.R.F. Leite, A.R. Malagutti, Simultaneous determination of ethionamide and pyrazinamide using poly (l-cysteine) film-modified glassy carbon electrode, Talanta 154 (2016) 197–207, https://doi.org/10.1016/j.talanta.2016.03.058.
[23] X. Yue, X. Xu, C. Liu, S. Zhao, Simultaneous determination of cefotaxime and nimesulide using poly (L-cysteine) and graphene composite modified glassy carbon electrode, Microchem. J. 174 (2022), 107058, https://doi.org/10.1016/j.microc.2021.107058.
[24] Q. Zhao, C. Wang, Y. Liu, J. Wang, Y. Gao, X. Zhang, T. Jiang, S. Wang, PEGylated mesoporous silica as a redox-responsive drug delivery system for loading thiol-containing drugs, Int. J. Pharm. 477 (1–2) (2014) 613–622, https://doi.org/10.1016/j.ijpharm.2014.10.056.
[25] S. Anantharaj, M. Jayakannan, Melt polycondensation approach for reduction degradable helical polyester based on l-cystine, J. Polym. Sci., Part A: Polym. Chem. 54(18) (2016) 2864-2875. https://doi.org/10.1002/pola.28172.
[26] A. Hoefling, D.T. Nguyen, Y.J. Lee, S.-W. Song, P. Theato, A sulfur–eugenol allyl ether copolymer: a material synthesized via inverse vulcanization from renewable resources and its application in Li–S batteries, Mater. Chem. Front. 1 (9) (2017) 1818–1822, https://doi.org/10.1039/C7QM00083A.
[27] E. Dokur, O. Gorduk, Y. Sahin, Differential pulse voltammetric determination of folic acid using a poly (cystine) modified pencil graphite electrode, Anal. Lett. 53 (13) (2020) 2060–2078, https://doi.org/10.1080/00032719.2020.1728540.
[28] T. Hezard, K. Fajerwerg, D. Evrard, V. Collière, P. Behra, P. Gros, Gold nanoparticles electrodeposited on glassy carbon using cyclic voltammetry: Application to Hg (II) trace analysis, J. Electroanal. Chem. 664 (2012) 46–52, https://doi.org/10.1016/j.jelechem.2011.10.014.
[29] S. Erden, Z. Yazan, A New Sepiolite Clay/TiO2/multiwall carbon nanotube modified carbon paste sensor for the adsorptive stripping square wave voltammetric analysis of vanillin in local food samples, Rev. Roum. Chim. 63 (2018) 977–986.
[30] J.D. Sawant, K.K. Patil, G.S. Gokavi, Kinetics and mechanism of oxidation of paracetamol by an Anderson-type 6-molybdocobaltate (III) in acidic medium, Transit. Met. Chem. 44 (2019) 153–159, https://doi.org/10.1007/s11243-018-0279-4.
[31] W.P. Silva, L.A. Silva, C.H. França, R.M. Sousa, R.A. Muñoz, E.M. Richter, Square-wave Voltammetric Determination of Propyphenazone, Paracetamol, and Caffeine: Comparative Study between Batch Injection Analysis and Conventional Electrochemical Systems, Electroanalysis 29 (8) (2017) 1860–1866, https://doi.org/10.1002/elan.201700160.
[32] D.E. Bayraktepe, Z. Yazan, Two-layered Au@Ag Bimetallic Nanocomposites-poly (L-Met) Platform for Highly Sensitive Chlorpheniramine Maleate Detection, Electroanalysis 34 (3) (2022) 445–454.
[33] L.U. Švorc, P. Tomčík, J. Svítková, M. Rievaj, D. Bustin, Voltammetric determination of caffeine in beverage samples on bare boron-doped diamond electrode, Food Chem. 135 (3) (2012) 1198–1204, https://doi.org/10.1016/j.foodchem.2012.05.052.
[34] B. Habibi, M. Jahanbakhshi, M. Abazari, A modified single-walled carbon nanotubes/carbon-ceramic electrode for simultaneous voltammetric determination of paracetamol and caffeine, J. Iran. Chem. Soc. 11 (2014) 511–521, https://doi.org/10.1007/s13738-013-0324-3.
[35] M. Tefera, A. Geto, M. Tessema, S. Admassie, Simultaneous determination of caffeine and paracetamol by square wave voltammetry at poly (4-amino-3-hydroxynaphthalene sulfonic acid)-modified glassy carbon electrode, Food Chem. 210 (2016) 156–162, https://doi.org/10.1016/j.foodchem.2016.04.106.
[36] I. Sadok, K. Tyszczuk-Rotko, A. Nosal-Wiercińska, Bismuth particles Nafion covered boron-doped diamond electrode for simultaneous and individual voltammetric assays of paracetamol and caffeine, Sens. Actuators B Chem. 235 (2016) 263–272, https://doi.org/10.1016/j.snb.2016.05.087.
[37] T.T. Minh, N.H. Phong, H. Van Duc, D.Q. Khieu, Microwave synthesis and voltammetric simultaneous determination of paracetamol and caffeine using an MOF-199-based electrode, J. Mater. Sci. 53 (4) (2018) 2453–2471, https://doi.org/10.1007/s10853-017-1715-0.
[38] T.Y. Feyisa, S.A. Kitte, D. Yenealem, G. Gebretsadik, Simultaneous electrochemical determination of paracetamol and caffeine using activated glassy carbon electrode, Anal. Bioanal. Electrochem. 12 (1) (2020) 93–106.
[39] M. Monteiro, E. Santos, D. Silva, C. Martínez-Huitle, E. Dos Santos, Simultaneous determination of paracetamol and caffeine in pharmaceutical formulations and synthetic urine using cork-modified graphite electrodes, J. Solid State Electrochem. 24 (2020) 1789–1800, https://doi.org/10.1007/s10008-020-04722-y.